Optimized grating as an ultra-narrow band absorber or plasmonic sensor

Lijun Meng,[1,2,3] Ding Zhao,[1,2] Zhichao Ruan,[1,3] Qiang Li,[1,2] Yuanqing Yang,[1,2] and Min Qiu[1,2,4,*]

[1]*State Key Laboratory of Modern Optical Instrumentation, Zhejiang University, Hangzhou 310027, China*

[2]*Department of Optical Engineering, Zhejiang University, Hangzhou 310027, China*

[3]*Department of Physics, Zhejiang University, Hangzhou 310027, China*

[4]*School of Information and Communication Technology, KTH Royal Institute of Technology, Electrum 229, 16440 Kista, Sweden*

**Corresponding author: minqiu@zju.edu.cn*

Received November 13, 2013; revised January 7, 2014; accepted January 10, 2014;
posted January 22, 2014 (Doc. ID 201261); published February 19, 2014

Lamellar gratings are investigated via temporal coupled-mode theory and numerical simulations. Total absorption can be achieved by an optimized grating with shallow grooves under normal incidence and the full width at half-maximum (FWHM) is only 0.4 nm. For certain wavelengths, the structure shows high absorption only within an ultra-narrow angle, which suggests that it can be used as a highly directional thermal emitter according to Kirchhoff's law. Besides, the resonant wavelength is sensitive to the refractive index of the environmental dielectric. The large sensitivity (1400 nm/RIU) and simultaneous small FWHM result in a huge figure-of-merit of 2300/RIU, which enables the structure to have great potential in plasmonic sensing.

OCIS codes: (050.2770) Gratings; (230.4555) Coupled resonators; (240.6680) Surface plasmons; (280.4788) Optical sensing and sensors.

http://dx.doi.org/10.1364/OL.39.001137

Structuring at microscale or nanoscale can transform metal surfaces from highly efficient reflectors to high-performance absorbers. Owing to its importance in both science and practical applications, the effect has been extensively studied in the past decade. Many absorbers based on different physical mechanisms have been proposed, and their potential applications have been demonstrated [1–15]. These absorbers can be generally categorized into two types in terms of their absorption bandwidths: broadband absorbers and narrowband absorbers. Narrowband absorbers are usually required in such fields as thermal radiation tailoring [16,17], sensitive detection, or sensing [5,11], etc. However, the reported bandwidths are typically above tens of nanometers and few studies have shown perfect absorbers with subnanometer bandwidths [18].

Although grating is an old structure [19], it remains a hot topic even to date. Both broadband and narrowband absorption can be realized by varying grating's composites and geometrical profiles [18,20–22]. Sharon *et al.* [18] proposed a grating-waveguide structure. A dielectric waveguide is superimposed on metal. Light confined in the waveguide is diffracted by grating upon it. A bandwidth of 0.1 nm is reported. As we know, surface plasmon polaritons (SPPs), which originate from collective oscillation of free electrons at metal-dielectric interface, are another form of surface wave. In [23], the authors designed a tungsten grating with shallow grooves, which is demonstrated as a highly directional thermal emitter. The similar structures can be also regarded as light absorbers. In this Letter, by directly constructing grating on a silver surface, a simpler absorber is designed with a subnanometer bandwidth. What's more, the resonant wavelength is easily tunable via geometrical scaling and ultrasensitive to the refractive index of the environmental dielectric. Its sensitivity and figure-of-merit (FOM) are 1400 nm/RIU and 2300/RIU, respectively.

The grating is superimposed on a substrate as illustrated in Fig. 1(a). Figure 1(b) shows its cross section of a unit cell, where s, h, and a represent half of the grating ridges, the depth of the grooves, and the period, respectively. Note that absorbers based on one-dimensional (1D) gratings are polarization-sensitive. However, absorbers based on two-dimensional (2D) crossed-gratings, extended from the 1D gratings as shown in Fig. 1(c), are polarization insensitive. Here, we focus mainly on the 1D gratings as the results for the 2D crossed-gratings are qualitatively similar. In the following numerical calculations using commercial software COMSOL MULTIPHYSICS based on finite element methods, right angles are modified to fillets, whose radii are $r = h/2$, to avoid singular points and to consider practical fabrication process. The silver permittivity is taken from the experimental data by Johnson and Christy [24]. For simplicity, only the TM wave (the magnetic field

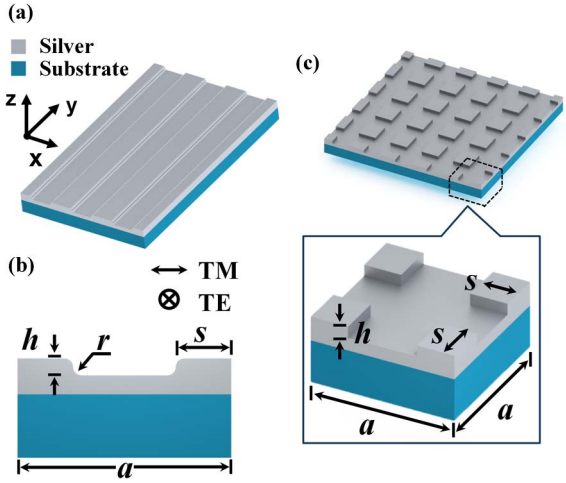

Fig. 1. (a) Schematic of the 1D grating. The grey region is silver and the blue region is the substrate. (b) Cross-section of a unit cell, s represents half of the grating ridges, h denotes the depth of the grooves, $r = h/2$ is the radius of the fillets, and a is the period. (c) 2D crossed-grating extended from 1D grating.

is parallel to the grooves) is considered here. Under light illumination with proper wavelength, SPPs will be excited. The energy of the excited surface wave is partially dissipated in metal as resistive heat described by resistive damping rate γ_{res}, and the other is coupled into free space in the form of radiation denoted by the radiative damping rate γ_{rad}. γ_{res} and γ_{rad} can be varied by adjusting the geometrical parameters of the grating. The radiation coupled from SPPs will interact with light directly reflected from the metal surface, which determines reflectance, therefore absorbance of the grating since the transmittance is zero. In the following, a time-saving approach based on temporal coupled-mode theory is first introduced and utilized to optimize geometrical parameters of the absorber. Then numerical simulations, which include incident light and require frequency scanning, are used to investigate the optimized absorber.

The temporal coupled-mode theory [25–27] provides an insightful analysis to the absorbance of nanostructure. In order to evaluate γ_{res} and γ_{rad}, we use the two-step method in [25,26]. We start with the lossless case by assuming the imaginary part of silver permittivity to be zero. Computed complex eigenfrequency $\omega_0 + i\gamma_{\mathrm{rad}}$ contains two parts, where ω_0 is the resonant angular frequency and γ_{rad} is the radiative damping rate. We then introduce metal loss by describing the silver with realistic permittivity. In this case, obtained complex eigenfrequency is $\omega_0 + i\gamma_{\mathrm{tot}}$, where γ_{tot} is the total damping rate, which includes both the radiative and the resistive damping rates. The resistive damping rate is then obtained from $\gamma_{\mathrm{res}} = \gamma_{\mathrm{tot}} - \gamma_{\mathrm{rad}}$. The absorbance at angular frequency ω is given by [27]:

$$A = \frac{4\gamma_{\mathrm{rad}}\gamma_{\mathrm{res}}}{(\omega - \omega_0)^2 + \gamma_{\mathrm{tot}}^2}. \tag{1}$$

Peak absorbance is $4\gamma_{\mathrm{rad}}\gamma_{\mathrm{res}}/\gamma_{\mathrm{tot}}^2$ at $\omega = \omega_0$. Critical coupling occurs when $\gamma_{\mathrm{rad}} = \gamma_{\mathrm{res}}$, leading to unity absorption ($A = 1$).

With grating period $a = 1400$ nm fixed, as illustrated in Figs. 2(a) and 2(b), the other geometrical parameters are varied around $s = 90$ nm and $h = 50$ nm, respectively, to demonstrate how the radiative and resistive damping rates evolve under normal incidence. Insets show the resonant wavelengths $\lambda = 2\pi c/\omega_0$ at each eigenmode. The corresponding peak absorbance and FWHMs are presented in Figs. 2(c) and 2(d). The critical coupling condition at $s = 92$ nm and $h = 50$ nm can be obtained when energy coupled to the eigenmode is totally dissipated in metal through resistive loss without reflection. It is attributed to the complete destructive interference between light coupled from SPPs and light directly reflected from a metal surface. The resonant wavelength is 1402 nm and the FWHM is only 0.4 nm. It can be observed from Fig. 2 that the ultra-narrow band and high absorption are insensitive to variation of geometrical profile. In the studied regimes, the peak absorbance remains higher than 80%, while the FWHMs stay under a half-nanometer. The resonant wavelength is also stable, not exceeding 2 nm relative to 1402 nm. All these features are of importance to practical fabrication and applications. The

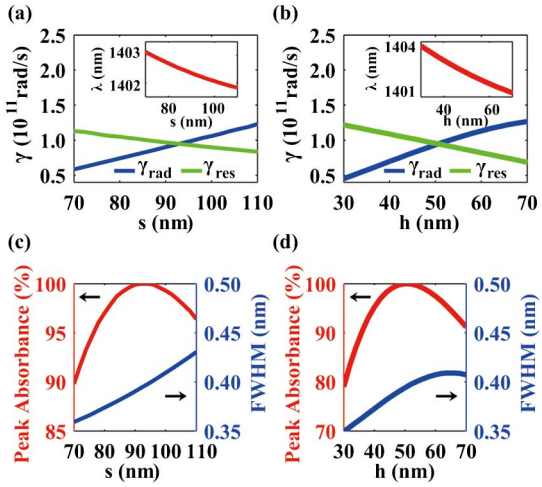

Fig. 2. Radiative (γ_{rad}) and resistive (γ_{res}) damping rates of the eigenmodes as functions of (a) half of the grating ridges s, and (b) the depth of the grooves h. Insets: the resonant wavelength at each eigenmode. Peak absorbance and FWHMs of the corresponding eigenmodes are presented in (c) and (d). If not particularly specified, $a = 1400$, $s = 92$, and $h = 50$ nm.

temporal coupled-mode theory used here provides a time-saving method to optimize absorbers.

We proceed to use numerical simulations to validate the perfect absorber. The solid-blue and dotted-red lines in Fig. 3(a) demonstrate that absorption spectra calculated based on two methods agree well with each other. To excite SPPs, the momentum provided by the grating ($\beta = k_0 \sin\theta + n2\pi/a$) should match the propagation constant of SPPs (k_{spp}), where θ is the angle of incidence, n is an integer, and a is the structure's period. Since shallow grooves are small perturbations to the flat interface, k_{spp} of the grating should be approximately equal to that of a flat interface between metal and dielectric. We found that for the normal incidence, $\theta = 0°$, when $n = 1$, $\beta = 2\pi/a$ agrees with the k_{spp} of a flat metal–air interface, which $k_{\mathrm{spp}} = 1.0034(2\pi/a)$ at 1402 nm. Considering $a = 1400$ nm and $\lambda_0 = 1402$ nm, the wave vector component along normal direction $k_z = \sqrt{k_0^2 - k_{\mathrm{spp}}^2}$ is almost zero. Therefore, the excited SPP field illustrated in Fig. 3(b)

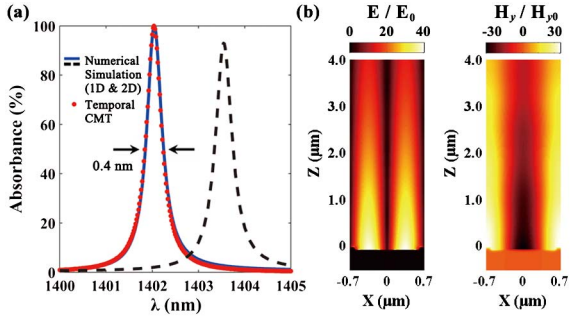

Fig. 3. (a) Computed absorption spectra of the optimized grating and the crossed-grating using the numerical simulation and the temporal coupled-mode theory. Blue-solid and black-dashed lines correspond to the 1D grating and the 2D crossed-grating, respectively. (b) Electric and magnetic enhancements at resonant wavelength (1402 nm). E_0 and H_{y0} are excitation fields, E and H_y are total fields.

does not exhibit field confinement. The field is distributed above the grating with a very slow decay and only a small proportion of electromagnetic field penetrates into the metal, which implies a very small resistive rate. So the total damping rate under critical coupling condition (twice the resistive damping rate) is ultra-small, resulting in ultra-narrow band light dissipation of the perfect absorber.

The absorption spectrum of the crossed-grating at normal incidence is also calculated and presented in Fig. 3(a). The geometrical parameters are the same as those of the optimized grating. One can observe that it shows only a small redshift. High absorption (93%) and ultra-narrow band (0.4 nm) still remain.

Absorption at oblique incidence is also studied and the spectra show abnormal characteristics. Figure 4(a) demonstrates absorptivity as functions of incident wavelength (λ) and angle of incidence (θ). Coordinates are transformed to photon energy (unit: eV) and wavenumber along the x axis. The grating can be assumed to be a form of 1D photonic crystal. Figure 4(a) displays a profile of its band diagram, and two photonic bandgaps around 0.9 and 1.3 eV can be seen. To intuitively show the absorptivity as a function of the angle of incidence, absorption spectra at two given wavelengths are plotted in Fig. 4(b). At 1900 nm, it shows near unity absorbance only within an ultra-narrow angle (0.4 mrad). As we know, absorption and emission are two reciprocal processes. According to Kirchhoff's law, the absorptivity and the emissivity of a surface are equal for polarized directional light at the same wavelength [28]. So the perfect absorber can be regarded as a thermal emitter. The angular pattern of emissivity under the same condition is the same as that of absorptivity as shown in Fig. 4(b). One can observe that for certain wavelengths (1900 nm) the emissivity at a particular angle (≈20°) is extremely large compared with that at other angles. Besides, the enhanced emissivity is only located within an ultra-small angular width (0.4 mrad), so it is a highly directional thermal emitter [23]. The narrow angular width is a signature of a large spatial coherence length ($l = \lambda/\theta = 2500\lambda = 4.75$ mm) at the corresponding wavelength, which suggests high monochromatic in the near field. The effect originates from thermally excited surface wave [29], which is in sharp contrast to the small spatial coherence length of the near field of blackbody [30]. Figure 4(b)

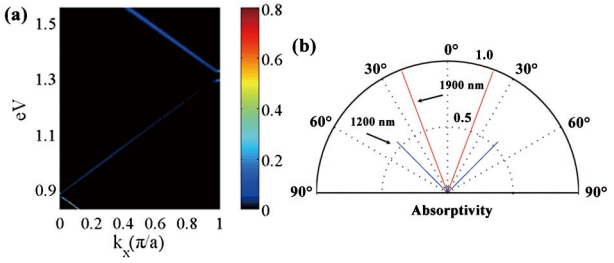

Fig. 4. (a) Absorption at oblique incidence. $k_x = (2\pi/\lambda)\sin\theta$, λ is incident wavelength and θ is angle of incidence. k_x is normalized with respect to π/a. Photon energy $E = hc/\lambda$, h is the Planck constant, and c is the light speed in vacuum. (b) Absorptivity angular patterns at 1900 and 1200 nm of the perfect absorber.

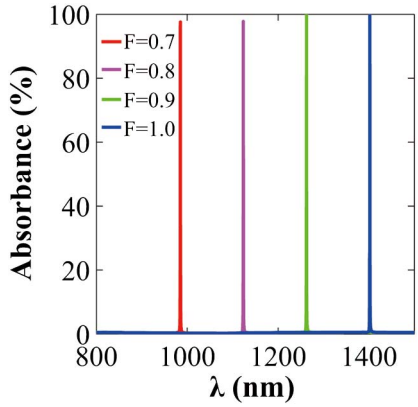

Fig. 5. Absorption spectrum as a function of geometrical scaling factor F.

shows another interesting phenomenon; the emitter radiates light with different wavelengths at distinct angles, which has potential application in wavelength division.

Until now we focused on the structure operating resonantly at approximately 1400 nm at normal incidence. Further simulations exhibit that it is geometrically scalable. Every geometrical parameter (a, s, h, and r) is multiplied by scaling factor F, which starts from 0.7 with a step of 0.1. The results are presented in Fig. 5. The peak can be tuned at a range of hundreds of nanometers, while the maximum absorbance remains above 97%, and FWHMs remain smaller than a half-nanometer.

It is well known that for plasmonic nanometallic structures, resonant wavelength depends on the refractive index of the environmental dielectric. The effect can be utilized to construct different types of plasmonic sensors [5,31,32], whose performances are usually described by sensitivity ($S = \Delta\lambda/\Delta n$) and figure-of-merit (FOM = S/FWHM). But the reported FOM are typically less than 1000/RIU in near infrared regime. Improving FOM by either increasing sensitivity or decreasing FWHM is still a challenge. In our simulations, the whole space over the absorber is filled by a dielectric with a refractive index n. Under normal illumination, dependence of absorption spectra on n is presented in Fig. 6(a). As n varies, the maximum absorptions remain near unity and FWHMs stay at 0.6 nm. The sensitivity is 1400 nm/RIU. Compared with a conventional absorber-based sensor, whose bandwidths are usually tens of nanometers, the bandwidth reported here is so small that the FOM can be as high

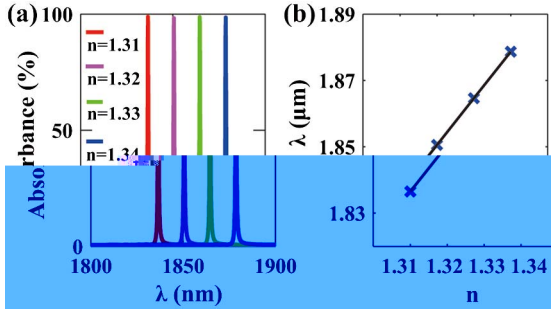

Fig. 6. Dependence of (a) absorption spectra and (b) resonant wavelengths on the refractive index of the environmental dielectric.

as 2300/RIU, paving the way for a highly sensitive plasmonic sensor. The peak wavelengths are extracted and plotted in Fig. 6(b), and good linearity is found. That is to say, the value of the variation of the peak wavelength divided by the variation of the refractive index is a constant.

It is worth noting that, in practice, it is inevitable that the incident light beam is composed of a range of incident angles, which will reshape the absorption spectra. Here the absorption spectrum with a Gaussian beam incidence is further investigated. In the simulations, the divergence of the Gaussian beam is chosen as 1°, and the waist of the beam is set at the very top of the structure. All other parameters are the same as those corresponding to the studied grating in Fig. 3(a). The result shows that although peak absorption drops from unity to about 55%, the FWHM remains only 0.4 nm, which will not degrade its performance in sensor applications.

In conclusion, a lamellar grating with shallow grooves is designed and investigated, which shows perfect absorption (100% absorbance) and ultra-narrow band (0.4 nm) dissipation under normal incidence. High absorption (93%) and ultra-narrow band (0.4 nm) maintain when extending the optimized 1D grating to 2D crossed grating. According to Kirchhoff's law, the perfect absorber can be considered as a highly directional thermal emitter with an angular width of 0.4 mrad at 1900 nm. The absorption spectra of the perfect absorber are highly sensitive to the refractive index of the environmental dielectric. The sensitivity and FOM are as high as 1400 nm/RIU and 2300/RIU, respectively. The structure presented here has great potential as a perfect absorber or high-performance plasmonic sensor.

This work is supported by the National Natural Science Foundation of China (Grant Nos. 61275030, 61205030 and 61235007), Qianjiang River Fellow Fund of Zhejiang Province, the Scientific Research Foundation for the Returned Overseas Chinese Scholars from the State Education Ministry, the Opened Fund of State Key Laboratory of Advanced Optical Communication Systems and Networks, the Fundamental Research Funds for the Central Universities, Doctoral Fund of Ministry of Education of China (Grant No 20120101120128), Zhejiang Provincial Funding for the Key Discipline of Optics, the Swedish Foundation for Strategic Research (SSF), and the Swedish Research Council (VR).

References

1. T. V. Teperik, F. J. García de Abajo, A. G. Borisov, M. Abdelsalam, P. N. Bartlett, Y. Sugawara, and J. J. Baumberg, Nat. Photonics **2**, 299 (2008).
2. X. Chen, H. Gong, S. Dai, D. Zhao, Y. Yang, Q. Li, and M. Qiu, Opt. Lett. **38**, 2247 (2013).
3. N. Bonod and E. Popov, Opt. Lett. **33**, 2398 (2008).
4. J. Hao, J. Wang, X. Liu, W. J. Padilla, L. Zhou, and M. Qiu, Appl. Phys. Lett. **96**, 251104 (2010).
5. N. Liu, M. Mesch, T. Weiss, M. Hentschel, and H. Giessen, Nano Lett. **10**, 2342 (2010).
6. J. Dai, F. Ye, Y. Chen, M. Muhammed, M. Qiu, and M. Yan, Opt. Express **21**, 6697 (2013).
7. S. Dai, D. Zhao, Q. Li, and M. Qiu, Opt. Express **21**, 13125 (2013).
8. K. Aydin, V. E. Ferry, R. M. Briggs, and H. A. Atwater, Nat. Commun. **2**, 517 (2011).
9. C. Wu, B. Neuner, J. John, A. Milder, B. Zollars, S. Savoy, and G. Shvets, Phys. Rev. B **84**, 075102 (2011).
10. X. Chen, Y. Chen, M. Yan, and M. Qiu, ACS Nano **6**, 2550 (2012).
11. S. Ogawa, K. Okada, N. Fukushima, and M. Kimata, Appl. Phys. Lett. **100**, 021111 (2012).
12. M. Yan, J. Opt. **15**, 025006 (2013).
13. L. Meng, D. Zhao, Q. Li, and M. Qiu, Opt. Express **21**, A111 (2013).
14. Y. H. Su, Y. F. Ke, S. L. Cai, and Q. Y. Yao, Light Sci. Appl. **1**, e14 (2012).
15. J. J. Talghader, A. S. Gawarikar, and R. P. Shea, Light Sci. Appl. **1**, e24 (2012).
16. X. Liu, T. Tyler, T. Starr, A. F. Starr, N. M. Jokerst, and W. J. Padilla, Phys. Rev. Lett. **107**, 045901 (2011).
17. M. D. Zoysa, T. Asano, K. Mochizuki, A. Oskooi, T. Inoue, and S. Noda, Nat. Photonics **6**, 535 (2012).
18. A. Sharon, G. Glasberg, D. Rosenblatt, and A. A. Friesem, J. Opt. Soc. Am. A **14**, 588 (1997).
19. R. W. Wood, Philos. Mag. **4**, 396 (1902).
20. E. Popov, D. Maystre, R. C. McPhedran, M. Nevère, M. C. Huthley, and G. H. Derrick, Opt. Express **16**, 6146 (2008).
21. V. G. Kravets, F. Schedin, and A. N. Grigorenko, Phys. Rev. B **78**, 205405 (2008).
22. A. Polyakov, S. Cabrini, S. Dhuey, B. Harteneck, P. J. Schuck, and H. A. Padmore, Appl. Phys. Lett. **98**, 203104 (2011).
23. M. Laroche, C. Arnold, F. Marquier, R. Carminati, J.-J. Greffet, S. Collin, N. Bardou, and J.-L. Pelouard, Opt. Lett. **30**, 2623 (2005).
24. P. B. Johnson and R. W. Christy, Phys. Rev. B **6**, 4370 (1972).
25. Z. Ruan and S. Fan, J. Phys. Chem. C **114**, 7324 (2010).
26. Z. Ruan and S. Fan, Phys. Rev. A **85**, 043828 (2012).
27. J. W. Yoon, K. H. Seol, S. H. Song, and R. Magnusson, Opt. Express **18**, 25702 (2010).
28. J.-J. Greffet and M. Nieto-Vesperinas, J. Opt. Soc. Am. A **15**, 2735 (1998).
29. J.-J. Greffet, R. Carminati, K. Joulain, J.-P. Mulet, S. Mainguy, and Y. Chen, Nature **416**, 61 (2002).
30. R. Carminati and J.-J. Greffet, Phys. Rev. Lett. **82**, 1660 (1999).
31. L. Zhang, C. Y. Chan, J. Li, and H. C. Ong, Opt. Express **20**, 12610 (2012).
32. W. Ma, J. Zhou, S. Huang, and H. Yuan, Chin. J. Lasers **38**, 0905008 (2011).